

An Investigation on Acoustic Wave Focalization by a Square Lattice Flat Lens

Serkan ALAGOZ

*Department of Physics, Inonu University
Malatya, Turkey; e-mail: serkan.alagoz@inonu.edu.tr*

(received April 29, 2011; accepted February 8, 2011)

A sonic crystal consists of a finite-size periodic array of scatters embedded in a background material. One of the fascinating properties of sonic crystals is the focusing phenomenon. In this study, the near field focusing effect of a solid-air 2D sonic crystal lens with a square lattice configuration is investigated in the second frequency band. The band structure and equifrequency contour of the crystal are analyzed to reveal the dispersion of an acoustic wave on the crystal structure. The frequency dependence of the acoustic wave focalization by the sonic crystal flat lens is demonstrated via Finite Difference Time Domain simulation results and experimental measurements.

Keywords: square lattice sonic crystal, wave focusing, plane-wave expansion method, FDTD simulation.

1. Introduction

One of the noteworthy applications of negative refraction is the development of flat lens structures that exhibit special focusing properties in certain frequency bands. A negative refraction behavior and imaging effect have been found firstly in photonic crystals (KOSAKA *et al.*, 1998; NOTOMI, 2000; LUO *et al.*, 2002; CUBUKCU *et al.*, 2003; ZHANG, LIU, 2004). These properties were then observed by using sonic crystals for acoustic waves (SANCHIS *et al.*, 2003; GARCIA *et al.*, 2003; GUPTA, YE, 2003). A sonic crystal consisting of a square array of rigid or liquid cylinders embedded in an air background was developed that have a negative-refraction behavior and imaging effect for acoustic waves (QIU *et al.*, 2005). It was shown theoretically and experimentally that the behavior of a sonic crystal lens could be described well by the lensmaker's formula (KUO, YE, 2004) making the sonic crystal slab a good candidate for the development of acoustic wave focusing devices to be utilized in acoustic imaging and audio technologies. There have not been much works considering the implementation of acoustic flat lenses in technology, yet. The investigation of focusing properties of flat lenses with various lattice types and the characterization of their features will contribute to the development of practical applications.

The far field focusing effect of a flat lens, which have triangular and honey comb lattice, have been studied

in many works (GUPTA, YE, 2003; QIU *et al.*, 2005; KUO, YE, 2004). In this study, authors have done an investigation on the near field focusing effect of acoustic waves in square lattice sonic crystals. The acoustic wave focalization effect was experimentally observed by a flat lens and its dependence on the wave frequency was revealed by numerical analyses and experimental measurements. The findings of the study contribute to the development of acoustic devices for acoustic wave focalization.

Sonic crystals are made of two-dimensional arrays of rigid cylinders placed in parallel in a medium (see Fig. 1). Rigid cylinders are called scatters. They scatter the acoustic wave inside the crystal slab and lead

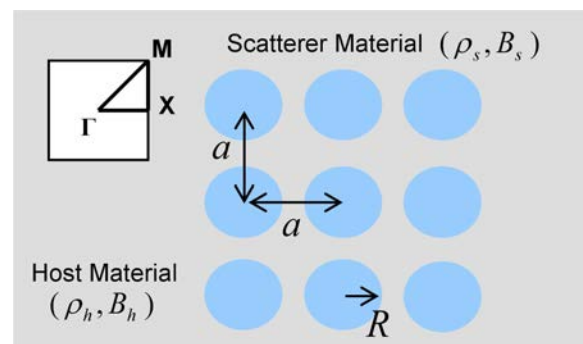


Fig. 1. The square lattice sonic crystal structure and related parameters.

a phenomenon, the so-called Bragg diffraction. Propagation of the waves in the host material will be modulated by the periodic structures of scatters and the dispersion of waves will no longer behave as in the homogenous medium. One of useful property observed in the squared lattice sonic crystal slab is the near field focalization effect, where a high intensity wave focalization region appears in the vicinity the crystal slab. In practice, such a high intensity region can be utilized for regional acoustic energy intensification and can find place in industrial and medical applications.

In this paper, the plane-wave expansion (PWE) method (KUO, YE, 2004; ECONOMOU, SIGALAS, 1993; SIGALAS, 1998; MIYASHITA, 2005; FENG *et al.*, 2005; PEREZ-ARJONA *et al.*, 2007) was used to obtain band structures characteristic of a square lattice flat lens in order to determine the frequency band, where the sonic crystal slab exhibit a negative effective refraction index (ERI). We observed that the self-collimation effect dominates the wave propagation inside the square lattice crystal at the lower bounds of the second band. However, this effect disappears at higher frequencies in the second band, when the wave focalization effect indicating a wave beam convergence becomes apparent. These analyses were confirmed via the Finite Difference Time Domain (FDTD) of simulation results and experimental measurements.

2. Numerical methods

2.1. The plane wave expansion method for band structure analysis of sonic crystals

The inhomogeneous wave equation for theoretical investigation of acoustic wave band structures was given in a normalized form (PEREZ-ARJONA *et al.*, 2007) as follows:

$$\frac{1}{\overline{B}(\mathbf{r})} \frac{\partial^2 p(\mathbf{r}, \tau)}{\partial \tau^2} - \nabla \cdot \left(\frac{1}{\overline{\rho}(\mathbf{r})} \nabla p(\mathbf{r}, \tau) \right) = 0, \quad (1)$$

where $p(\mathbf{r}, \tau)$ is sound pressure, $\overline{\rho}(\mathbf{r})$ is the normalized density, $\overline{\rho}(\mathbf{r}) = \frac{\rho(\mathbf{r})}{\rho_h}$, and $\overline{B}(\mathbf{r})$ represents the normalized bulk modulus, $\overline{B}(\mathbf{r}) = \frac{B(\mathbf{r})}{B_h}$. (ρ_h, B_h) are density and bulk modulus of the host material; the ($\rho(\mathbf{r}), B(\mathbf{r})$) parameters are used for describing the inhomogeneous medium, respectively; τ is the normalized time expressed as $\tau = c_h t$ (PEREZ-ARJONA *et al.*, 2007). The speed of sound in the host material was denoted by c_h . The second-order inhomogeneous differential equation given by Eq. (1) well defines the acoustic wave propagation in the sonic crystal slab and was solved to obtain the band structure (KUO, YE, 2004; MIYASHITA, 2005; FENG *et al.*, 2005; PEREZ-ARJONA *et al.*, 2007). For the solution, a harmonic form for the sound pressure

$p(\mathbf{r}, \tau) = p(\mathbf{r})e^{iw\cdot\tau}$ was assumed. Then, Eq. (1) can be rearranged as,

$$\frac{w^2}{\overline{B}(\mathbf{r})} p(\mathbf{r}) + \nabla \cdot \left(\frac{1}{\overline{\rho}(\mathbf{r})} \nabla p(\mathbf{r}) \right) = 0. \quad (2)$$

Applying the Floquet–Bloch theorem for the periodic system, the spatial function of the pressure is described by $p(\mathbf{r}) = p_{\mathbf{k}}(\mathbf{r})e^{i\mathbf{k}\cdot\mathbf{r}}$, where $p_{\mathbf{k}}(\mathbf{r})$ is a periodic function according to the periodicity of the sonic crystal. Equation (2) was solved for the periodic function $p(\mathbf{r})$ by the PWE method (ECONOMOU, SIGALAS, 1993; SIGALAS, 1998; MIYASHITA, 2005). For this purpose, the $p(\mathbf{r})$, $\overline{\rho}(\mathbf{r})$ and $\overline{B}(\mathbf{r})$ periodic functions were expanded in Fourier series with the coefficients of $b_{\mathbf{G}}$, $\rho_{\mathbf{G}}$ and $p_{\mathbf{k}}$ (ECONOMOU, SIGALAS, 1993; SIGALAS, 1998; MIYASHITA, 2005):

$$\overline{\rho}(\mathbf{r})^{-1} = \sum_{\mathbf{G}} \rho_{\mathbf{G}}^{-1} e^{i\cdot(\mathbf{G}\cdot\mathbf{r})}, \quad (3)$$

$$\overline{B}(\mathbf{r})^{-1} = \sum_{\mathbf{G}} b_{\mathbf{G}}^{-1} e^{i\cdot(\mathbf{G}\cdot\mathbf{r})}, \quad (4)$$

$$p(\mathbf{r}) = e^{i(\mathbf{k}\cdot\mathbf{r})} \sum_{\mathbf{G}} p_{\mathbf{k},\mathbf{G}} e^{i\cdot(\mathbf{G}\cdot\mathbf{r})}, \quad (5)$$

where \mathbf{k} is a two-dimensional Bloch vector restricted to the first Brillouin zone and \mathbf{G} is the 2D reciprocal lattice vector. For a square lattice, it is written in the form of $\mathbf{G} = (2\pi/a)(n_1\mathbf{e}_1 + n_2\mathbf{e}_2)$, where n_1 and n_2 are integers.

Equation (2) was transformed into a finite matrix equation using Fourier series as (MIYASHITA, 2005; FENG *et al.*, 2005; PEREZ-ARJONA *et al.*, 2007):

$$\sum_{\mathbf{G}'} [w^2 b_{\mathbf{G}-\mathbf{G}'}^{-1} - \rho_{\mathbf{G}-\mathbf{G}'}^{-1} (\mathbf{k}+\mathbf{G})(\mathbf{k}+\mathbf{G}')] p_{\mathbf{G}'} = 0 \quad (6)$$

By solving Eq. (6), w_n eigenvalues were obtained for $n = 1, 2, 3, \dots$ to draw the band structures of the sonic crystal. In the Eq. (6), the $b_{\mathbf{G}}$ and $\rho_{\mathbf{G}}$ coefficients for the periodic cylindrical structure shown in Fig. 2 were written in the form of (PEREZ-ARJONA *et al.*, 2007):

$$\rho_{\mathbf{G}}^{-1} = \begin{cases} \underline{\rho} f_r + (1 - f_r) & \mathbf{G} = 0 \\ (\underline{\rho} - 1) F(\mathbf{G}) & \mathbf{G} \neq 0 \end{cases}, \quad (7)$$

$$b_{\mathbf{G}}^{-1} = \begin{cases} \underline{B} f_r + (1 - f_r) & \mathbf{G} = 0 \\ (\underline{B} - 1) F(\mathbf{G}) & \mathbf{G} \neq 0 \end{cases}, \quad (8)$$

where $f_r = \frac{\pi \cdot R^2}{a^2}$ is the filling ratio of the square lattice sonic crystal for the R radius of cylinders, and $\underline{\rho} = \rho_h/\rho_s$ and $\underline{B} = B_h/B_s$. (ρ_s, B_s) are the density and bulk modulus of the host material. The function $F(\mathbf{G})$ is called the structuring factor and calculated by:

$$F(\mathbf{G}) = 2 f_r \frac{J_1(|\mathbf{G}| R)}{|\mathbf{G}| R}, \quad (9)$$

where $J_1(x)$ is the Bessel function of the first kind of order one (PEREZ-ARJONA *et al.*, 2007).

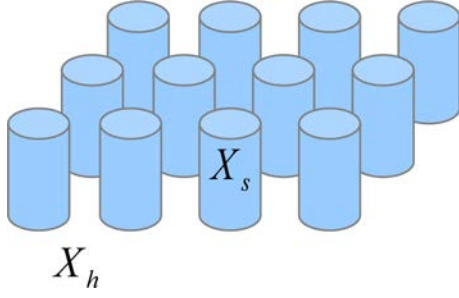


Fig. 2. Infinite Periodic cylindrical structure with (X_h, X_s) two levels of material parameter.

2.2. The finite difference time domain method for acoustic wave simulation

Sound waves are described by the following simple equations (MIYASHITA, 2005).

$$\frac{\partial \mathbf{v}}{\partial \tau} = -\underline{\rho} \nabla p, \quad \frac{\partial p}{\partial \tau} = -\overline{B} \nabla \cdot \mathbf{v}, \quad (10)$$

where \mathbf{v} denotes the normalized particle velocity expressed as $\mathbf{v} = \rho_h c_0 \mathbf{V}$. The material parameters of crystal structures are described by the normalized medium density, $\underline{\rho} = \rho_h / \rho_s$, and the normalized bulk modulus, $\overline{B} = \underline{B}^{-1} = B_s / B_h$.

To obtain an FDTD based numerical solution of (10), the following discrete finite difference formulas (MIYASHITA, 2005) were employed in the acoustic wave propagation simulation:

$$v_x^{n+\frac{1}{2}} \left(i + \frac{1}{2}, j \right) = v_x^{n-\frac{1}{2}} \left(i + \frac{1}{2}, j \right) - \underline{\rho} \left(i + \frac{1}{2}, j \right) R_x [p^n(i+1, j) - p^n(i, j)], \quad (11)$$

$$v_y^{n+\frac{1}{2}} \left(i, j + \frac{1}{2} \right) = v_y^{n-\frac{1}{2}} \left(i, j + \frac{1}{2} \right) - \underline{\rho} \left(i, j + \frac{1}{2} \right) R_y [p^n(i, j+1) - p^n(i, j)], \quad (12)$$

$$p^{n+1}(i, j) = p^n(i, j) - \overline{B}(i, j) R_x \cdot \left[v_x^{n+\frac{1}{2}} \left(i + \frac{1}{2}, j \right) - v_x^{n+\frac{1}{2}} \left(i - \frac{1}{2}, j \right) \right] - \overline{B}(i, j) R_y \left[v_y^{n+\frac{1}{2}} \left(i, j + \frac{1}{2} \right) - v_y^{n+\frac{1}{2}} \left(i, j - \frac{1}{2} \right) \right], \quad (13)$$

where R_x and R_y are defined as $R_x = \frac{\Delta u}{\Delta x}$ and $R_y = \frac{\Delta u}{\Delta y}$ and set to $R_x = 0.35$ and $R_y = 0.35$ for a stable wave propagation. The spatial sampling points of the two-dimensional FDTD method given for Eqs. (11), (12) and (13) are shown in Fig. 3.

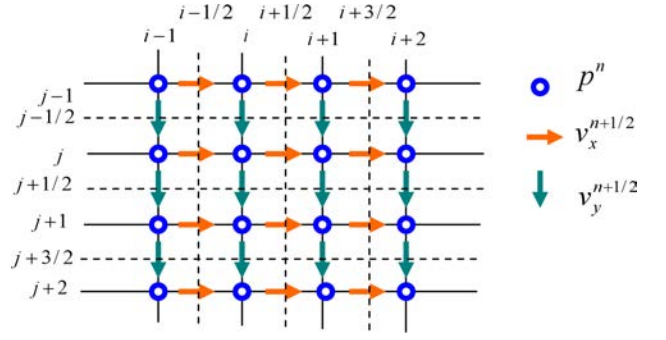


Fig. 3. Spatial sampling points for the two-dimensional FDTD method.

3. Experimental setup

Two dimensional square lattice sonic crystal is fabricated as an 14×14 array of aluminum rods with a periodic lattice constant of 2.5 cm and a cylinder radius of 1 cm. The filling ratio of the crystal structure (f_r) is 0.50. The density and bulk modulus of the aluminum rods used in experiments are 2700 kg/m^3 and $7.0 \cdot 10^{10} \text{ kg/m} \cdot \text{s}^2$, respectively. The heights of the rods are 32 cm.

Intensity distribution maps were obtained by scanning the two dimensional measurement zone seen in Fig. 4. The experiment set is composed of an automated measurement zone, an input-output system (a signal conditioner, a digital-analog converter and an amplifier) and a computer for controlling all measurement processes. In the automated measurement zone, intensity measurements of the acoustic waves are done by scanning the $40 \times 56 \text{ cm}^2$ measurement zone in 0.5 cm steps.

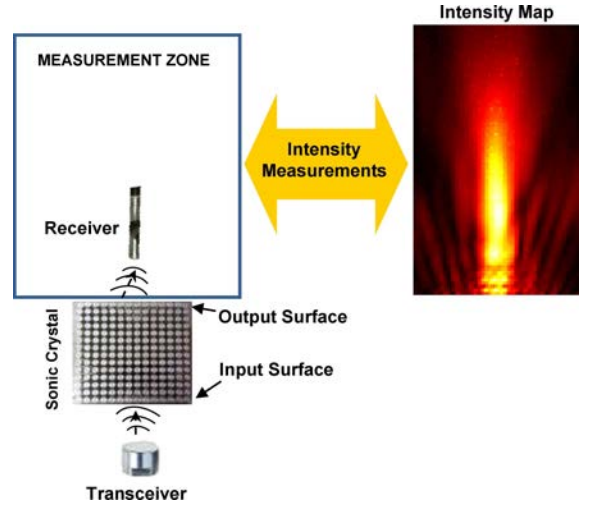


Fig. 4. Experimental setup.

4. Results and discussions

The band structure and Equifrequency contours (EFC) obtained for the aluminum rod square lattice

crystal with the material parameters $\underline{\rho} = 4.8 \cdot 10^{-4}$, $\underline{B} = 2.1 \cdot 10^{-6}$ are illustrated in Figs. 5a and 5b. Being convex around the Γ point in the second band suggest that the squared rod sonic crystal refracts negatively the incident waves. In the second band, the sonic

crystal slab behaves as an acoustic metamaterial due to $\mathbf{k} \cdot \mathbf{V}_g < 0$. This condition implies that the group velocity \mathbf{V}_g and wave vectors \mathbf{k} are opposite in direction, which is a common accepted sign of negative refraction properties on a band structure analysis.

Figure 5c illustrates negative ERI estimation of the second band, which is calculated using the formula of $n = -|\mathbf{k}|c_h/w_{\mathbf{k}}$, where the norm of wave vectors, $|\mathbf{k}|$, and the corresponding frequency value, $w_{\mathbf{k}}$, are obtained from the second band Equipfrequency surface (EFS) characteristics of the sonic crystal. As illustrated in Fig. 5c, the sonic crystal can accomplish a negative refraction index in the range of $[-0.3, -0.9]$ at the low frequency region (band of 0.62–0.75) of the second band. The sonic crystal slab can operate as a flat lens in this frequency range. Dashed contours in Fig. 5c indicate EFCs at the normalized frequency of 0.62 and 0.75. The refraction index in Fig. 5c indicates an apparent variation over the EFCs; this implies that the refraction index of the square lattice sonic crystal deviates with respect to the beam direction at a constant frequency. This is a factor deterring single spot super resolution of wave focusing by the square lattice crystal.

The flat character (Rectangular form) of EFC appearing at the lower bound of the second band indicates the existence of a self-collimation effect (KOSAKA *et al.*, 1999; CICEK *et al.*, 2011). As illustrated in Fig. 6a, a flat EFS surface results in the parallel group velocity vectors ($\mathbf{V}_g = \nabla_{\mathbf{k}}w$) and leads to wave beams being almost parallel inside the sonic crystal as sketched in Fig. 6b. As the frequency increases, EFC forms in rather round shape; this indicates a wave beams convergence effect that leads to wave focalization as illustrated in Fig. 6c.

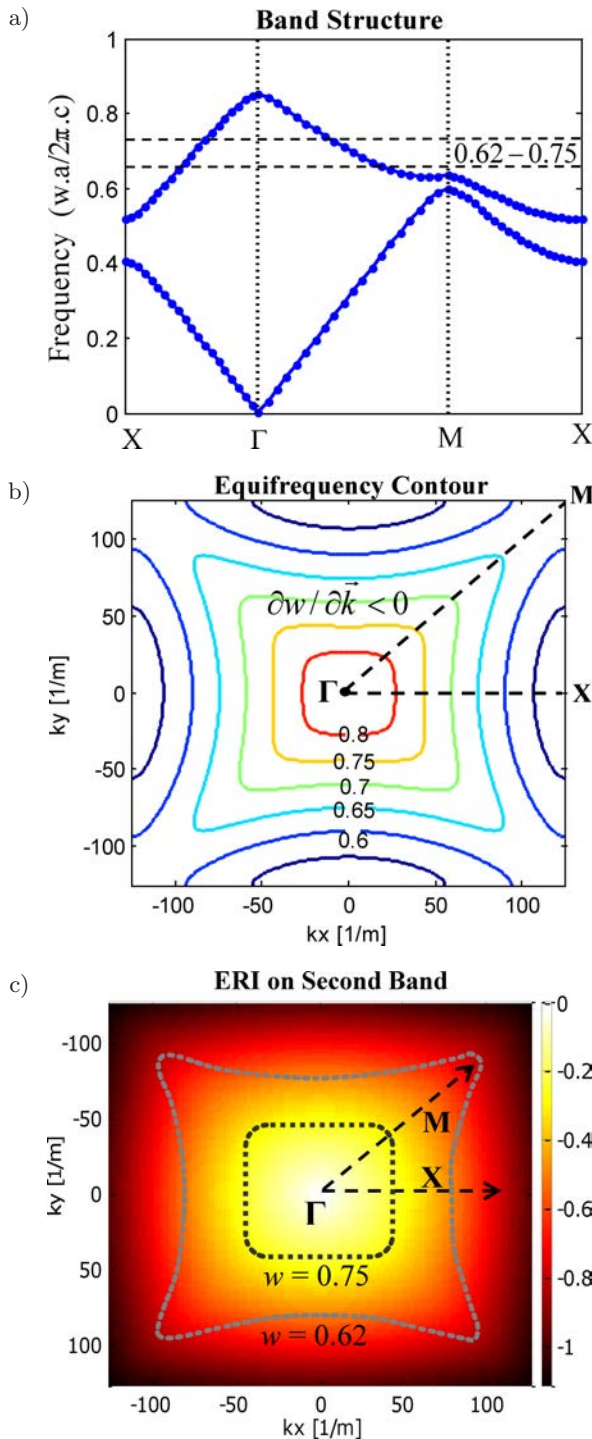


Fig. 5. Band structure in (a), EFC in (b) and ERI in (c) of the second frequency band for the squared lattice sonic crystal. Lattice constant $a = 25$ mm, scatterer radius $r = 10$ mm, filling ratio $f_r = 0.50$ and speed of sound $c_h = 340$ m/sn.

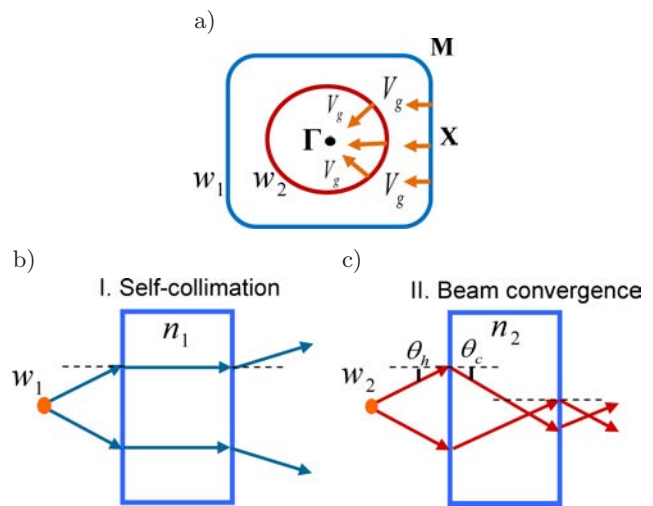


Fig. 6. a) Group velocity vectors on the second band EFCs. Wave frequencies and refraction indexes satisfy $w_2 > w_1$ and $0 > n_2 > n_1$, b) a ray-trace representation of the self-collimation effect, c) a ray-trace representation of the beam convergence effect.

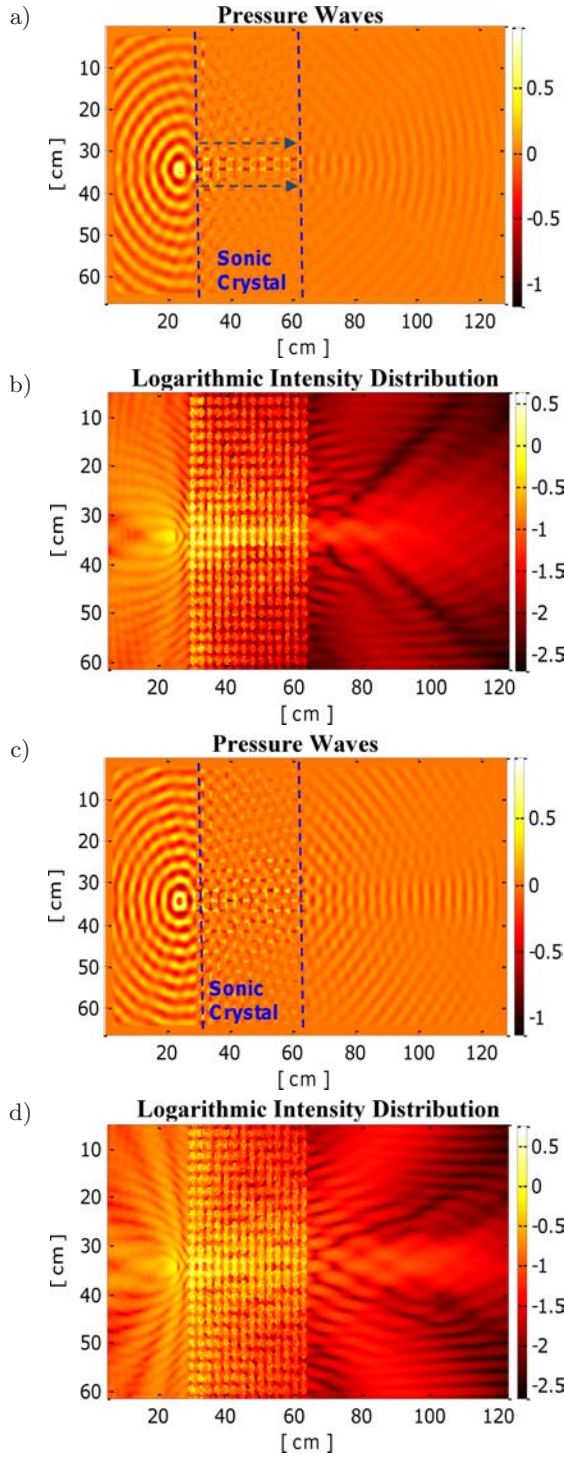


Fig. 7. The pressure field pattern (p) in (a) and (c) and the logarithmic intensity distribution ($\log_{10}(p^2)$) in (b) and (d) from the FDTD simulation. Lattice constant $a = 25$ mm, scatterer radius $r = 10$ mm, filling ratio $f_r = 0.50$ and speed of sound $c_h = 340$ m/sn. Frequency of wave source is 9200 Hz in (a)–(b) and 9900 Hz in (c)–(d).

Figure 7 shows FDTD simulation results of the acoustic flat lens made of the sonic crystal used in the experiment. Figures 7a and 7b demonstrate the self-collimation effect obtained at 9200 Hz (normal-

ized frequency of 0.67). In accordance to Fig. 6b, the waves propagate along the crystal almost parallel as if in a wave-guide. Figures 7c and 7d show a wave focalization region in the vicinity of the output surface of the flat lens at 9900 Hz. The focalization region is composed of a gathering of several focusing points. This is so because the EFC of the sonic crystal does not perfectly match with the circular EFC of the air. This prevents focusing all refracted wave beams into a single focal spot due to considerable variation at the refraction index depending on the beam direction. In previous works, hexagonal EFC forms of triangular lattice sonic crystals were shown to provide a better matching with the circular EFC and all-angle negative refraction (AANR). Hence, triangular lattice crystal gives a superior wave focusing effect called “ideal imaging” or “super-resolution” to be employed in acoustic imaging applications (QIU *et al.*, 2005; ALAGOZ *et al.*, 2009; ROBILLARD *et al.*, 2011)

In Fig. 8a, the experimental intensity map picture obtained for a monochromatic wave source with the

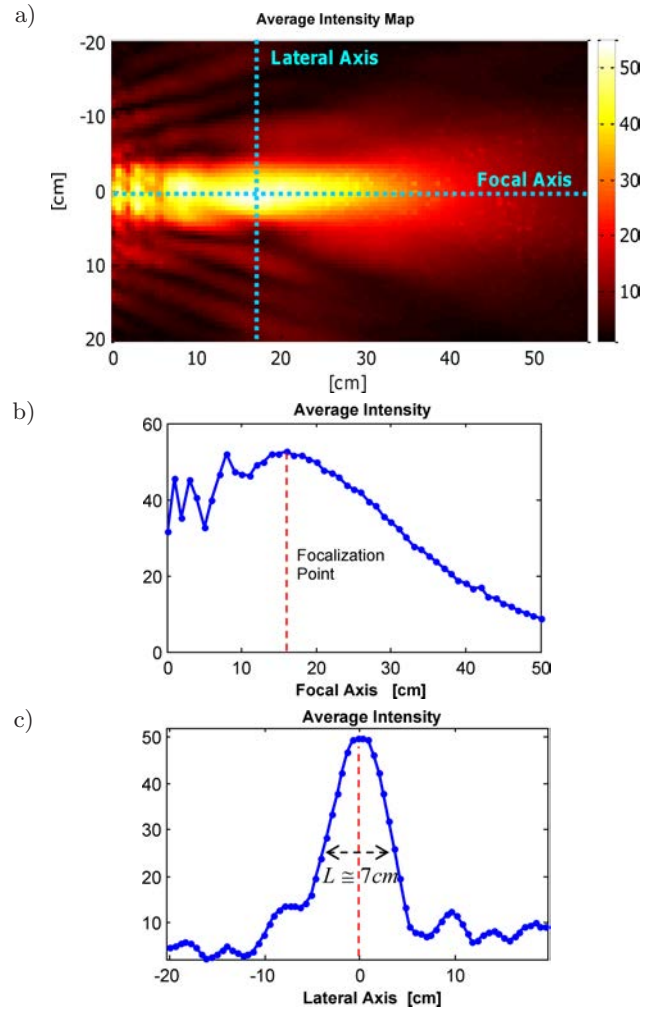


Fig. 8. Intensity map (a) obtained for the experimental sonic crystal slab at 9900 Hz, intensity versus-focal axis plots (b) and intensity versus-lateral axis (c).

frequency of 9900 Hz (normalized frequency of 0.72) demonstrates a near field wave focalization effect of the sonic crystal in the second frequency band. A peak intensity on the focal axis was obtained at a distance of roughly 17 cm away from the flat lens as illustrated in Fig. 8b. The peak intensity distribution along the lateral axis was shown in Fig. 8c. The level of the peak intensity of wave focalization is noticeably high comparing to peripheral peaks around the focusing point, which implies that the flat lens exhibits a considerable wave focalization for a point wave source with frequency of 9900 Hz. However, the focusing point observed is in the diffraction limits because the size at half maximum (L) equals about two wavelengths (2λ). The authors did not observe a sub-wavelength focusing effect via the tested sonic crystal. Although it is not efficient for a high resolution acoustic imaging application, it might be beneficial to acoustic energy transmission applications (KASAI *et al.*, 2011).

The frequency dependence of the negative refraction was demonstrated in previous works (QIU *et al.*, 2005; JIA, ZHANG, 2007; ALAGOZ *et al.*, 2009). This strong dependence on the wave frequency makes also the focusing phenomenon of a flat lens strongly dependent on the frequency of the acoustic wave source. Figure 9a reveals the intensity distribution on the focal axis for a frequency range of 8500–10200 Hz with a 100 Hz step (normalized frequency 0.62–0.75) in the second frequency band of the experimental square lattice flat lens. In the point of practical applications, the peak intensity of focalization and distances of the focalization points from the flat lens are the important parameters. Figure 9b shows the intensity distribution on the focal axis at four frequencies. The intensity distributions obtained at 9900 Hz and 10200 Hz show the focusing point peaks resulting from the convergence of the negative refracted beams in accordance with Fig. 6c. The intensity distribution measured for 9200 and 9500 does not exhibit any wave focalization peak due to the self-collimation effect illustrated in Fig. 6b. As shown in Figs. 9a and 9b, the maximum intensity can be obtained on the output surface of a flat lens at the frequency of 9500 Hz. As the frequency increases, while the focusing point moved away from the surface of flat lens, the peak intensity of focusing point decreased. This shows that the square lattice flat lens provides the strongest wave focalization on the surface of the flat lens owing to the nearest beam converge at this output surface. For triangular lattice flat lenses, which were known to provide the far field focusing, the maximum peak intensity of focusing points can be obtained at more distant locations from the surface of flat lens (QIU *et al.*, 2005; ALAGOZ *et al.*, 2009). Preferably, this makes the square lattice flat lenses a suitable candidate for the near field wave energy transmission applications.

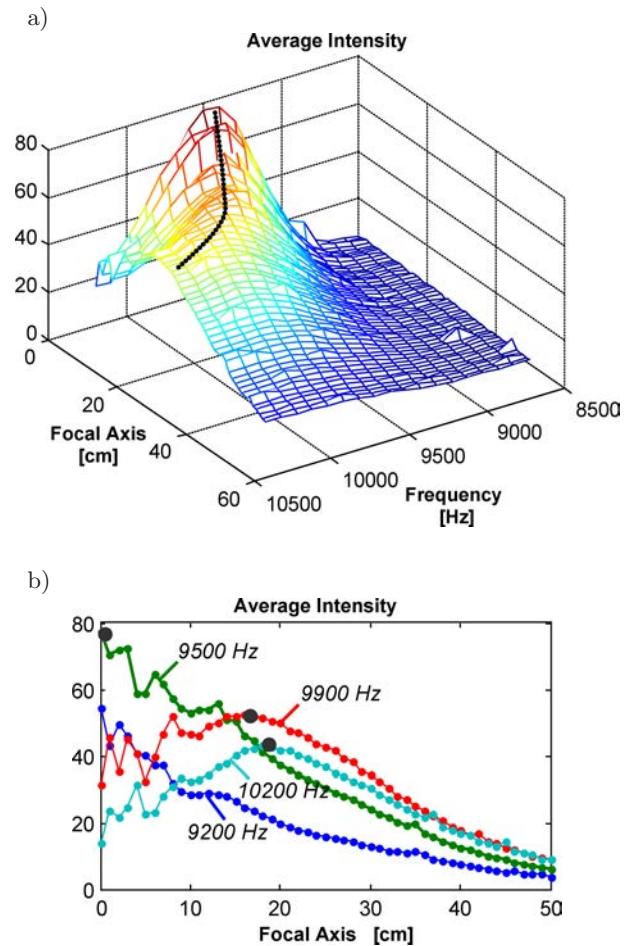


Fig. 9. a) Measured intensity distribution versus focal axis and wave frequency from 8500 Hz to 10200 Hz, b) measured intensity distribution versus focal axis for selected frequencies 9200 Hz (normalized 0.67), 9500 Hz (normalized 0.69), 9900 Hz (normalized 0.72) 10200 Hz (normalized 0.75). Dashed line in (a) indicates the peak intensity regarding to the focal axis.

5. Conclusions

The wave focusing effect of the flat lens made of a two-dimensional square lattice sonic crystal were investigated in the second frequency band. At the lower bounds of the second band, the self-collimation effect dominated the wave propagation owing to the flat EFC. However, when the frequency exceeded the normalized frequency of 0.69 (9500 Hz), wave convergences were observed to overcome the self-collimation effect due to the slightly rounding of the EFC lines. The authors observed that the square lattice flat lens was capable of forming a strong wave energy focalization region in the near field of the crystal slab. In the implementation of acoustic devices requiring a strong near field energy focalization square lattice flat lenses can be more suitable than triangular lattice sonic crystals. However, a subwavelength focusing or super-resolution effect similar to the triangular lattice

flat lens (QIU *et al.*, 2005; ROBILLARD *et al.*, 2011) were not observed as in the squared lattice flat lens.

The group velocity vector analysis of the EFC surface is helpful to explain the wave propagation in the sonic crystals. Parallelization of group velocity vectors on the EFC indicates that the self-collimation effect dominates the wave propagation inside the crystal, whereas the convergence of group velocity vectors imply a wave beam convergence inside the sonic crystal. The FDTD simulation results and experimental measurements confirm these effects appearing in the second band of square lattice sonic crystal.

The frequency dependence of the focalization property of a square lattice flat lens was shown experimentally. The highest wave intensity was measured on the output surface of the flat lens at 9500 Hz. As frequency increases, the peak intensity moved further from the surface of flat lens.

The findings of this paper will be helpful in the development of acoustic energy transmission devices.

References

1. ALAGOZ S., ALAGOZ B.B. (2009), *Frequency-controlled wave focusing by a sonic crystal lens*, Applied Acoustics, **70**, 1400–1405.
2. CICEK A., KAYA O.A., ULUG B. (2011), *Wide-band all-angle acoustic self-collimation by rectangular sonic crystals with elliptical bases*, J. Phys. D: Appl. Phys., **44**, 205104.
3. CUBUKCU E., AYDIN K., OZBAY E., FOTEINOPOULOU S., SOUKOULIS C.M. (2003), *Negative refraction by photonic crystals*, Nature, **423**, 604.
4. ECONOMOU E.N., SIGALAS M.M. (1993), *Classical wave propagation in periodic structures: Cermet versus network topology*, Phys. Rev. B, **48**, 13434–13438.
5. FENG L., LIU X.P., CHEN Y.B., HUANG Z.P., MAO Y.W., CHEN Y.F., ZI J., ZHU Y.Y. (2005), *Negative refraction of acoustic waves in two-dimensional sonic crystals*, Phys. Rev. B, **72**, 033108.
6. GARCIA N., NIETO-VESPERINAS M., PONIZOVSKAYA E.V., TORRES M. (2003), *Theory for tailoring sonic devices: Diffraction dominates over refraction*, Phys. Rev. E, **67**, 046606.
7. GUPTA B., YE Z. (2003), *Theoretical analysis of the focusing of acoustic waves by two dimensional sonic crystals*, Phys. Rev. E, **67**, 036603.
8. JIA W., ZHANG S. (2007), *Strongly frequency-dependent negative refraction of a two-dimensional sonic crystal wedge*, Physics Letters A, **372**, 721–724.
9. KASAI Y., TSURUTA K., FUJIMORI K., FUKANO H., NOGI S. (2011), *Negative Refraction and Energy-Transmission Efficiency of Acoustic Waves in Two-Dimensional Phononic Crystal: Numerical and Experimental Study*, Jpn. J. Appl. Phys., **50**, 067301.
10. KOSAKA H., KAWASHIMA T., TOMITA A., NOTOMI M., TAMAMURA T., SATO T., KAWAKAMI S. (1998), *Superprism phenomena in photonic crystals*, Phys. Rev. E, **58**, R10096-R10099.
11. KOSAKA H., KAWASHIMA T., TOMITA A., NOTOMI M., TAMAMURA T., SATO T., KAWAKAMI S. (1999), *Self collimating phenomena in photonic crystals*, Appl. Phys. Lett., **74**, 1212–4.
12. KUO C.H., YE Z. (2004), *Sonic crystal lenses that obey the lensmaker's formula*, J. Phys. D: Appl. Phys., **37**, 2155–2159.
13. LUO C., JOHNSON S.G., JOANNOPOULOS J.D., PENDRY J.B. (2002), *All-angle negative refraction without negative effective index*, Phys. Rev. B, **65**, 201104-1201104-4.
14. MIYASHITA T. (2005), *Sonic crystals and sonic waveguides*, Meas. Sci. Technol., **16**, R47–R63.
15. NOTOMI M. (2000), *Theory of light propagation in strongly modulated photonic crystals: Refraction like behavior in the vicinity of the photonic band gap*, Phys. Rev. B, **62**, 1069610705.
16. PEREZ-ARJONA I., SANCHEZ-MORCILLO V.J., REDONDO J., ESPINOSA V., STALIUNAS K. (2007), *Theoretical prediction of the nondiffractive propagation of sonic waves through periodic acoustic media*, Phys. Rev. B, **75**, 014304.
17. QIU C., ZHANG X., LIU Z. (2005), *Far-field imaging of acoustic waves by a two-dimensional sonic crystal*, Phys. Rev. B, **71**, 054302.
18. ROBILLARD J.F., BUCAY J., DEYMIER P.A., SHELKE A., MURALIDHARAN K., MERHEB B., VASSEUR J.O., SUKHOVICH A., PAGE J.H. (2011), *Resolution limit of a phononic crystal superlens*, Phys. Rev. B, **83**, 224301.
19. SANCHIS L., HAKANSSON A., CERVERA F., SANCHEZ-DEHESA J. (2003), *Interferometers based on two dimensional arrays of rigid cylinders in air*, Phys. Rev. B, **67**, 035422.
20. SIGALAS M.M. (1998), *Defect states of acoustic waves in a two-dimensional lattice of solid cylinders*, J. Appl. Phys., **84**, 3026–3030.
21. ZHANG X.D., LIU Z. (2004), *Negative refraction of acoustic waves in two-dimensional phononic crystals*, Appl. Phys. Lett., **85**, 341.